Hindawi
Scientific Programming
Volume 2021, Article ID 7323654, 10 pages
https://doi.org/10.1155/2021/7323654

Research Article

Computed Tomography Image Based on Intelligent Segmentation Algorithm in the Diagnosis of Ovarian Tumor

Ling Zhu[1] **Yucheng He**[2] **Nan He**[3] **and Lanhua Xiao**[1]

[1]*Department of Gynecological Oncology Surgery, Chenzhou No. 1 People's Hospital (The First Affiliated Hospital of Xiangnan University), Chenzhou 423000, Hunan, China*
[2]*Medical Imaging Center, Chenzhou No. 1 People's Hospital (The First Affiliated Hospital of Xiangnan University), Chenzhou 423000, Hunan, China*
[3]*Department of Urology Surgery, Chenzhou No. 1 People's Hospital (The First Affiliated Hospital of Xiangnan University), Chenzhou 423000, Hunan, China*

Correspondence should be addressed to Lanhua Xiao; 2013012425@stu.zjhu.edu.cn

Received 28 August 2021; Revised 17 October 2021; Accepted 20 October 2021; Published 13 November 2021

Academic Editor: Gustavo Ramirez

This study was to explore the application of computed tomography (CT) images based on intelligent segmentation algorithms in the analysis of ovarian tumors, so as to provide a theoretical basis for clinical diagnosis of ovarian tumors. In this study, 100 patients with ovarian tumors were selected as the research objects and performed CT imaging examinations; a convolutional neural networks (CNN) algorithm model was constructed and applied to CT diagnostic image segmentation of patients with ovarian tumors, so as to analyze the effectiveness of the proposed algorithm for CT image segmentation. As a result, the image was segmented three times under the CNN algorithm, and the numbers of true positives (TP) were 50, 49, and 50, respectively; the numbers of false positives (FP) were 1, 2, and 1, respectively; the numbers of false negatives (FN) were 2, 3, and 2, respectively; and the numbers of true negatives (TN) were 47, 46, and 47, respectively. Thus, there was no great difference in the three measured values ($P \geq 0.05$). The accuracy of the CNN algorithm was 0.97, 0.95, and 0.97, respectively, for the three times of segmentation; the precision was 0.98, 0.96, and 0.98, respectively; the recall was 0.96, 0.94, and 0.96, respectively. Thus, the accuracy, precision, and recall of the three measurements were not greatly different ($P \geq 0.05$). In addition, the $F1$ values of three measurements were 0.97, 0.94, and 0.97, respectively, which all were close to 1, showing no statistically great difference ($P \geq 0.05$). The segmentation accuracy, precision, and recall of the algorithm in this study were greatly greater than the SE-Res Block U-shaped CNN algorithm, and the density peak clustering algorithm, and the differences were statistically significant ($P < 0.05$). In short, the CNN algorithm showed high accuracy, precision, recall, and comprehensive evaluation values for CT image segmentation, which made the diagnosis of malignant or benign ovarian tumors more effective and provided reliable theoretical guidance for clinical analysis of ovarian tumors.

1. Introduction

Ovarian tumor refers to tumor that occur on the ovaries and is one of the common genital tumors in women. Ovarian tumors have a high incidence in nonbirth women, early menarche or late menopause [1], and the incidence of women decreases with the increase in the number of childbirths. Based on this, there is a theory that ovulation causes damage to ovarian epithelial cells; repeated damage and repair processes may promote cancer, and most cases are caused by autosomal dominant inheritance. According to histopathology, ovarian tumor can be divided into two types: benign ovarian tumor and evil ovarian tumor [2]. Among them, benign ovarian tumors account for about 75% of ovarian tumors; most of them are cystic, with uniform density, clear borders, smooth surfaces, cyst walls, and thin separation rules [3] and no wall nodules; 85%–90% of ovarian tumors have various types and are generally solid or cystic, with uneven density distribution [4].

Clinical imaging methods for breast tumors usually include magnetic resonance (MRI), ultrasound, and computed tomography (CT) [5]. Transvaginal ultrasound

(TVUS) uses ultrasound echo to transmit imaging images, which can help identify potential ovarian hyperplasias and determine whether they are solid hyperplasias or cysts. It is fast, economical, noninvasive, and reproducible. However, the morphology, internal structure, and relationship with surrounding tissues of smaller ovarian masses are often unclear, and it is difficult to detect solid tumors with a diameter of less than 1 cm. MRI soft tissue shows high resolution, multiplane imaging, and is noninvasive. It is very advantageous in observing the depth of endometrial lesions invading the muscle layer and the boundary between cervical tumors and the bladder or rectum, but the overall cost is too high. CT scan scans the abdomen through special X-rays, allowing doctors to see the various parts of the abdomen and pelvis, which can locate and characterize pelvic tumors, and learn whether the liver, lungs, and retroperitoneal lymph nodes have metastasis, with fast scanning time and clear image [6].

In clinical medicine, in order to meet the needs of disease diagnosis and treatment, patients are scanned [7], so as to know the condition of each patient's internal organs. Before the application of intelligent segmentation algorithms, this process was almost done independently by doctors. Experienced doctors have higher judgment accuracy, but because the training of doctors is expensive and time consuming [8], and after the training is completed, they will suffer from unavoidable limitations such as energy and mood fluctuations [9], resulting in the accuracy of judgment, showing high instability [10]. Intelligent segmentation algorithms are often used in medical image analysis at this stage to assist diagnosis and reduce the probability of misdiagnosis. Medical image segmentation mainly deals with the segmentation of various images involved in the medical field, such as common electronic computer tomography CT images. Its main task is to segment regions of interest, such as tumors, from these medical images [11]. Different from the common segmentation tasks in daily life, medical images will have problems such as low contrast, low signal-to-noise ratio, and low light intensity due to the influence of image acquisition equipment [12]; organs have individual differences and are subject to movement deformation. These factors make it difficult to segment medical images. Deep learning algorithms have characterization learning capabilities [13], and it can classify input information according to its hierarchical structure. The algorithm categories can be divided into three categories: convolutional neural network (CNN), which is often used for image data analysis and processing; recurrent neural network (referred to as RNN) for text analysis or natural language processing; and generative adversarial network (GAN for short) used for data generation or nonsupervised learning applications [14]. The CNN model shows excellent feature extraction capabilities, avoiding the limitations of manually extracting features. That is to say, CNN has good classification performance, can solve a major problem in image recognition, and has good performance in image segmentation.

In summary, the use of deep learning neural network models to enhance the processing of medical images is a hot research topic. Therefore, 100 cases of ovarian tumor patients undergoing CT examination were selected as the research samples, and the CNN target detection algorithm was adopted to segment the patient's CT image. The segmentation accuracy, precision, and recall of the algorithm were compared to discuss the segmentation based on deep learning. The diagnostic value of the algorithm's CT images for ovarian tumors was expected to provide corresponding data reference for the clinical evaluation of ovarian cancer.

2. Materials and Methods

2.1. Research Objects and Grouping. In this study, 100 patients with ovarian tumor were treated in the hospital from January 2017 to January 2019. The patients were all female, aged 22–45 years old. The patients included in the study had undergone pathological examinations and CT imaging examinations before surgery. This study had been approved by the Ethics Committee of hospital. The patient and his family members had a more detailed understanding of the content and methods of the study, and they agreed to sign the relevant informed consent.

The inclusion criteria were determined as follows: patients aged between 18 and 45 years old; patients diagnosed with ovarian tumor by pathological and CT imaging examinations; patients who had not been treated with other drugs in the study recently; and patients not received radiotherapy and chemotherapy.

The exclusion criteria were defined as follows: patients with mental illness or unconsciousness; female patients who had not given birth; patients with incomplete clinical history data; and patients who did not cooperate with treatment.

2.2. CT Examination. The ovarian tumor items were registered on the CT machine according to the CT number, name, gender, and age of the subject on the CT sheet, and check whether the registration content was consistent with the application sheet. The number of exposures and time should be minimized to complete the scanning requirements, thereby reducing the patient's radiation dose and save money, not to do meaningless scanning. After scanning, it had to browse the reconstructed CT images to confirm that there were no missing scans and that the images of all layers meet the diagnostic requirements and then perform the imaging operation. After the above operations were completed, the patient was required to enter the scanning room to exit the bed, lower the height of the bed, and get off the scanning bed. Two full-time oncology doctors were invited to conduct double-blind reading of CT images and record the results. If there was any disagreement, a third experienced doctor was required to perform the interpretation.

2.3. Image Segmentation Based on CNN Intelligent Algorithm. In the past, neural networks were almost full connections between layers, as shown in Figure 1. The method used by CNN was partial connection, as shown in Figure 2, which can reduce complexity and effectively adjust overfitting. The weight sharing can make the model generalize and reduce learning rules, as shown in Figure 3.

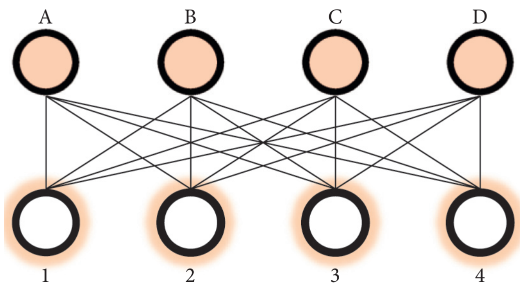

Figure 1: Fully connected neural network.

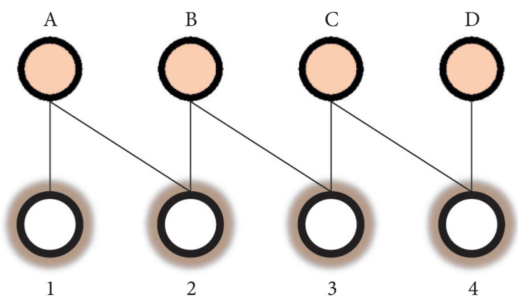

Figure 2: Convolution connection.

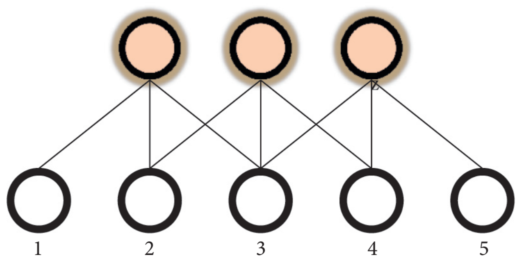

Figure 3: Weight sharing.

The feature of its translation invariance was that it can grasp the most important features, filter the irrelevant parameters, and reduce the complexity to facilitate calculations (as shown in Figure 4); in addition, when the pixel was slightly displaced in the neighborhood, the output was unchanged, the robustness was enhanced, and it had a certain anti-interference effect. The three applications of the CNN algorithm are shown in Figure 5.

The earliest representative neural network was the LetNet model. Although its scale was small, it was completed including a fully connected layer, a convolutional layer, and a pooling layer. The input image was a 28 ∗ 28 grayscale image, which was then convolutional pooled twice to become 50 ∗ 4 ∗ 4, and then a hidden layer fully connected network was used to complete the classification. Since the beginning of LetNet, the field of deep learning had developed rapidly, and convolutional network technology had become more and more mature. Figure 6 shows the LetNet model.

In CNN, the backpropagation (BP) algorithm is generally used for tasks such as image segmentation, and it can update the parameters and weights continuously. Input: 100 picture samples, the number of layers of the CNN model L and the types of all hidden layers. For the convolutional layer, the size of the convolution kernel was set to K, the dimension of the convolution kernel submatrix was set to F, and the padding size and the stride were defined as P and S, respectively. For the pooling layer, the pooling area size k and the pooling standard (MAX or average) had to be defined. In addition, the gradient iteration parameters iteration step size α, maximum iteration number MAX, and stop iteration threshold ε had to be defined, too. Output: the parameter matrix W and bias b of each hidden layer and output layer of the CNN model. BP algorithm is by far the most used neural network algorithm. When neuron j was iterating n, the output signal error was defined as follows:

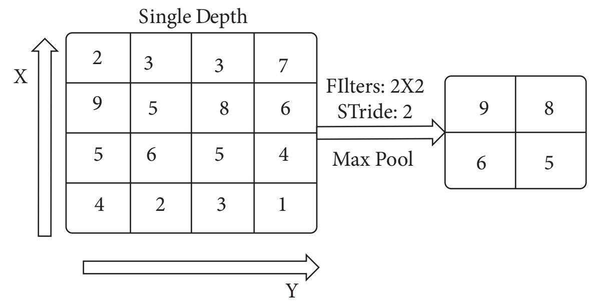

Figure 4: Maximum pooling.

$$e_j(n) = d_j(n) - y_j(n). \tag{1}$$

In the above equation, the neuron j was the output node.

The error energy of neuron j instantaneously was defined as $(1/2)e_j^2$. Correspondingly, the instantaneous value of the entire error energy $\varepsilon(n)$ was the sum of the instantaneous values of the neuron error energy of the output layer, so the calculation formula of $\varepsilon(n)$ is given as follows:

$$\varepsilon(n) = \frac{1}{2}\sum_{j\in c} e_j^2(n). \tag{2}$$

Set C included all neurons in the output layer of the network. N was denoted to be the total number of patterns included in the training set. Finding the sum of $\varepsilon(n)$ for all n and normalize the size of the set can get the mean square error energy, expressed as the following equation:

$$\varepsilon_{av} = \frac{1}{N}\sum_{n=1}^{N} \varepsilon(n). \tag{3}$$

Equation (3) depicted that neuron j was fed by a set of functional signals generated by the layer of neurons to its left, so the induced local domain $v_j(n)$ generated at the input of the activation function of neuron j was expressed as follows:

$$v_j(n) = \sum_{i=0}^{m} w_{ji}(n) y_j(n), \tag{4}$$

m in the above equation referred to the number of all inputs acting on neuron j. The synapse weight $w_{ji}(n)$ was equal to the bias bj of neuron j. Then, the function signal $y_j(n)$ that

(a) (b) (c)

Figure 5: The three applications of the CNN algorithm. (a) Classification. (b) Object detection. (c) Semantic segmentation.

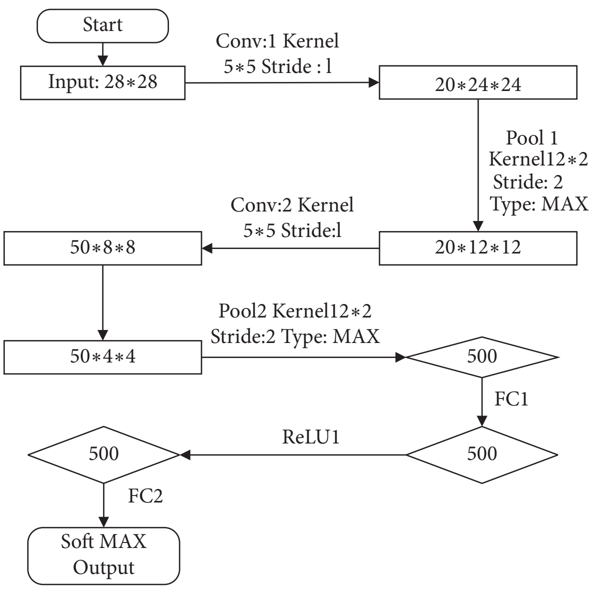

Figure 6: Work flow chart of LetNet neural network.

appeared at the output of neuron j during iteration n was given below:

$$y_j(n) = \left(\varphi v_j(n)\right). \tag{5}$$

In a similar way to the LMS algorithm, a correction value $\Delta w_{ji}(n)$ was applied to the synapse weight $w_{ji}(n)$, which was proportional to the edited derivative of $\varepsilon(n)$ to $w_{ji}(n)$ $(\partial\varepsilon(n)/\partial w_{ji}(n))$. According to the chain rule of calculus, this gradient can be expressed as below equation:

$$\frac{\partial\varepsilon(n)}{\partial w_{ji}(n)} = \frac{\partial\varepsilon(n)}{\partial e_j(n)}\frac{\partial e_j(n)}{\partial y_j(n)}\frac{\partial y_j(n)}{\partial v_j(n)}\frac{\partial v_j(n)}{\partial w_{ji}(n)}. \tag{6}$$

The partial derivative $\partial\varepsilon(n)/\partial w_{ji}(n)$ represented a sensitive factor, which determined the search direction of the synapse weight $w_{ji}(n)$ in the weight space.

The following equation could be obtained by differentiating $e_j(n)$ on both sides of equation (2):

$$\frac{\partial\varepsilon(n)}{\partial e_j(n)} = e_j(n). \tag{7}$$

Equation (8) could be obtained by differentiating $y_j(n)$ on both sides of equation (1):

$$\frac{\partial e_j(n)}{\partial y_j(n)} = -1. \tag{8}$$

Next, $v_j(n)$ on both sides of equation (5) can be differentiated to obtain the below equation:

$$\frac{\partial y_j(n)}{\partial v_j(n)} = \left(\varphi_j' v_j(n)\right). \tag{9}$$

Finally, taking the differentiation of $w_{ji}(n)$ on both sides of equation (4), we can get the following equation:

$$\frac{\partial v_j(n)}{\partial w_{ji}(n)} = y_j(n). \tag{10}$$

Substituting equations (7)~(10) into equation (6), we can get the following equation:

$$\frac{\partial\varepsilon(n)}{\partial w_{ji}(n)} = -e(n)\varphi_j'\left(v_j(n)\right)y_j(n). \tag{11}$$

Applied to $w_{ji}(n)$, the modified $\Delta w_{ji}(n)$ was defined by the delta rule as follows:

$$\Delta w_{ji}(n) = -\eta\frac{\partial\varepsilon(n)}{w_{ji}(n)}. \tag{12}$$

where η in the above equation referred to the learning rate parameter of the BP algorithm. The use of the negative sign in equation (12) meant that the gradient dropped in the weight space, then equation (11) was substituted into equation (12), and below equation could be obtained.

$$\Delta w_{ji}(n) = \eta\delta_j(n)y_i(n). \tag{13}$$

The local gradient $\delta_j(n)$ in equation above was defined as follows:

$$\delta_j(n) = -\frac{\partial\varepsilon}{\partial v_j(n)} = -\frac{\partial\varepsilon}{\partial e_j(n)}\frac{\partial e_j(n)}{\partial y_j(n)}\frac{\partial y_j(n)}{\partial v_j(n)} = e_j(n)\varphi_j'\left(v_j(n)\right). \tag{14}$$

The local gradient indicated the required change in synaptic weights. According to equation (14), the local gradient $\delta_j(n)$ of the output neuron j was equal to the product of the corresponding error signal $e_j(n)$ of the neuron and the derivative $(v_j(n))$ of the corresponding activation function.

2.4. Evaluation Indicators. In this study, accuracy was used to represent the proportion of all predictions that were correct. The specific calculation method was shown in equation (15); Precision meant that all predictions were the ratio of positive examples where the actual labels were positive examples, and the specific calculation method was shown in equation (16). Recall was the ratio at which the positive sample was found, which could be calculated with equation (17).

$$A = \frac{\mathrm{TN} + \mathrm{TP}}{\mathrm{TN} + \mathrm{TP} + \mathrm{FP} + \mathrm{FN}}, \quad (15)$$

$$P = \frac{\mathrm{TP}}{\mathrm{TP} + \mathrm{FP}}, \quad (16)$$

$$R = \frac{\mathrm{TP}}{\mathrm{TP} + \mathrm{FN}}. \quad (17)$$

In the above equations, A, P, and R referred accuracy, precision, and recall, respectively; TP refers to true positive, which meant the prediction result was positive, and the actual result was positive; FP refers to false positive, which meant that the prediction result was positive, but the actual result was negative; FN refers to false negative, which meant that the prediction result was negative, but the actual result was positive; and TN refers to true negative, which meant that the prediction result was negative, and the actual result was negative.

$$F = \frac{\left(\alpha^2 + 1\right) P * R}{\alpha^2 (P + R)},$$
$$F1 = \frac{2P * R}{P + R}, \quad (18)$$

where α was a constant and P and R indicators sometimes appear contradictory, so they need to be considered comprehensively. The most common method is F-Measure (weighted harmonic average of precision and recall). When the parameter $\alpha = 1$, it is the common $F1$, which combines the results of P and R. When the $F1$ is higher, the experimental method is more effective.

2.5. Statistical Analysis. The data processing of this experiment was analyzed using SPSS 19.0 version of statistical software. The measurement data were expressed by means $\pm$ standard deviation ($\overline{x} \pm s$), and the counting of quantitative data was expressed by percentage (%) and concentration. Data analysis indicated that the difference was statistically significant with $P < 0.05$.

3. Results

3.1. CT Images of Ovarian Tumor. Figure 7 shows the CT images of three random patients with ovarian tumors. It can be seen that the ovarian tumor was round. Figures 7(a)–7(c) show images of all malignant tumors, which were solid or cystic, with uneven density distribution.

3.2. Analysis of Intelligent Segmentation Algorithms Model. Based on the results interpreted by three clinically experienced doctors, 52 out of 100 patients with ovarian tumor were malignant and 48 were benign tumors. Malignant tumors were defined as positive cases, and benign tumors were defined as negative cases. On this basis, the CNN algorithm was used to interpret the data three times. Figure 8 shows the data of TP, FP, FN, and TN. As illustrated in the figure, there was no significant difference among the three positive and negative cases ($P \geq 0.05$).

Figure 9 shows the accuracy of the CNN algorithm calculated based on positive and negative cases, indicating that all predictions were correct; precision indicated the proportion of all predicted malignant tumors that were actually labeled as malignant tumors; recall was the rate at which malignant tumors were found. As shown in Figure 9, the accuracy, precision, and recall of the three measurements were not significantly different ($P \geq 0.05$).

3.3. Comprehensive Evaluation of Intelligent Segmentation Algorithm Model. The comprehensive evaluation of a single index was not high. F-measure was used for comprehensive evaluation of the data. The larger the value of F, the higher the effectiveness of the algorithm model. As shown in Figure 10, the F value measured by the CNN algorithm three times was close to 100%, indicating that the algorithm model was very effective, and the difference among the three data was not remarkable ($P \geq 0.05$).

3.4. Comparison on Segmentation Performance between the Algorithm in This Study and Traditional Algorithms. The SE-Res Block U-shaped CNN algorithm and the density peak clustering algorithm were introduced to compare with the algorithm in this study. The results are shown in Figure 11. The segmentation accuracy, precision, and recall of the algorithm in this study were significantly greater than those of the SE-Res Block U-shaped CNN algorithm and the density peak clustering algorithm, and the differences were statistically significant ($P < 0.05$).

The segmentation and reconstruction results of ovarian cancer CT images of the three algorithms were further compared, and the results are illustrated in Figure 12. It revealed that the segmentation and reconstruction of the algorithm in this study showed higher definition and lower noise, and the overall presentation quality was better than that of the SE-Res Block U-shaped CNN algorithm and the density peak clustering algorithm, which were consistent with the above quantitative results.

4. Discussion

Ovary is a pair of substantial organs located in the female pelvis, and it belongs to the female sex glands. In order to produce egg cells and ovulate, it secretes sex hormones to promote the development and maintenance of female sexual characteristics [15]. The appearance of human changes with age. The surface of the young girl is smooth and uneven due to multiple ovulations after adolescence; the maximum

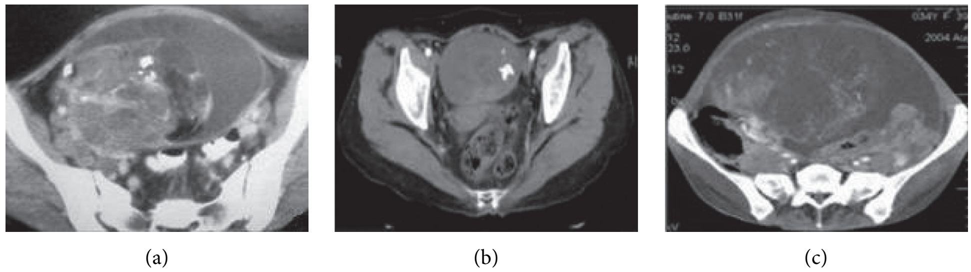

Figure 7: CT images of ovarian tumor. Note: (a) a huge cystic solid mass in the pelvic cavity, with a large amount of soft tissue and a small amount of fat and scattered calcifications. (b) The shadow of a round mixed density mass on the anterior upper part of the uterus, with uneven density, and strip-shaped calcifications can be seen inside. (c) A cystic solid space on both sides of the ovary, a large amount of ascites, and thickened peritoneum.

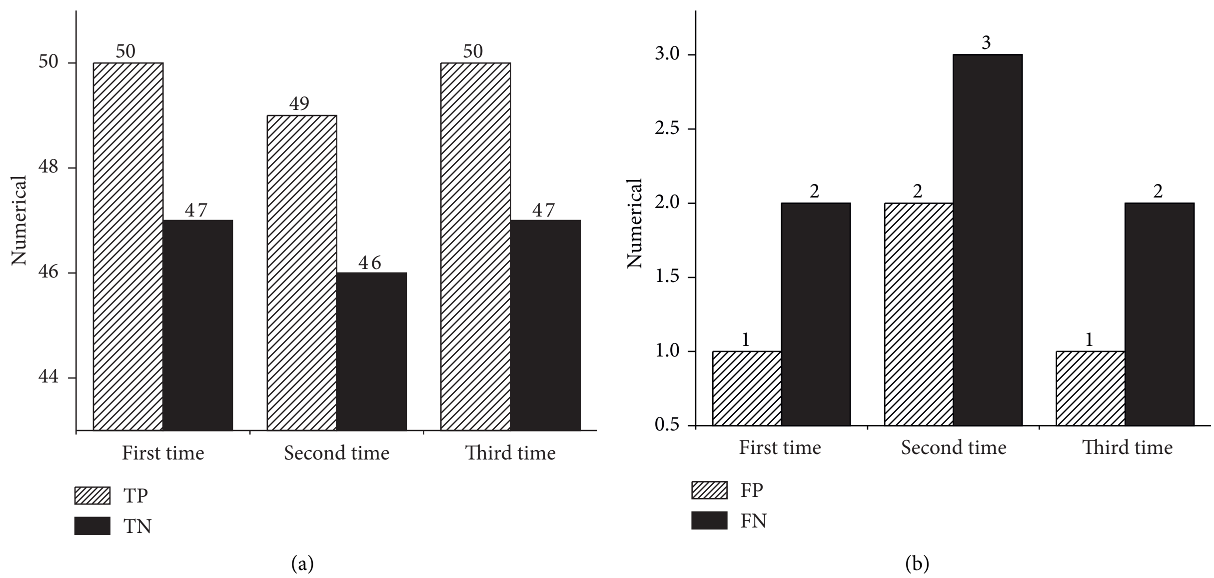

Figure 8: The data of TP, FP, FN, and TN. *Note.* (a) The data of TP and TN; (b) The data of FP and FN.

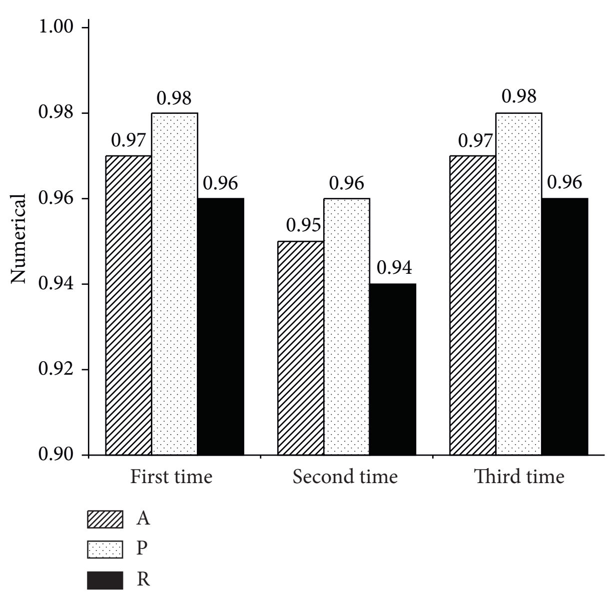

Figure 9: The accuracy, precision, and recall.

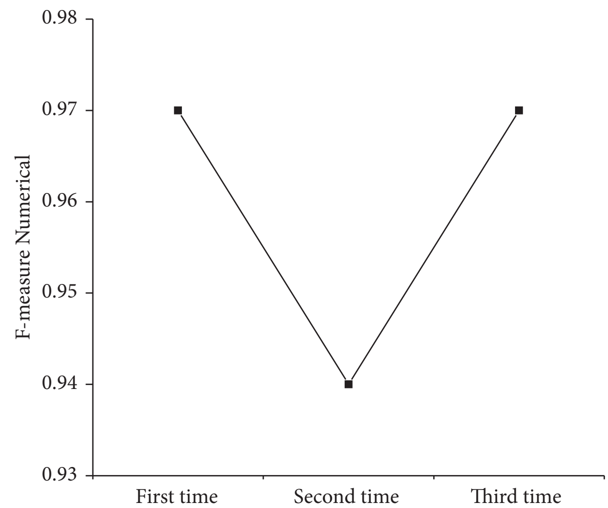

Figure 10: Results of comprehensive evaluation.

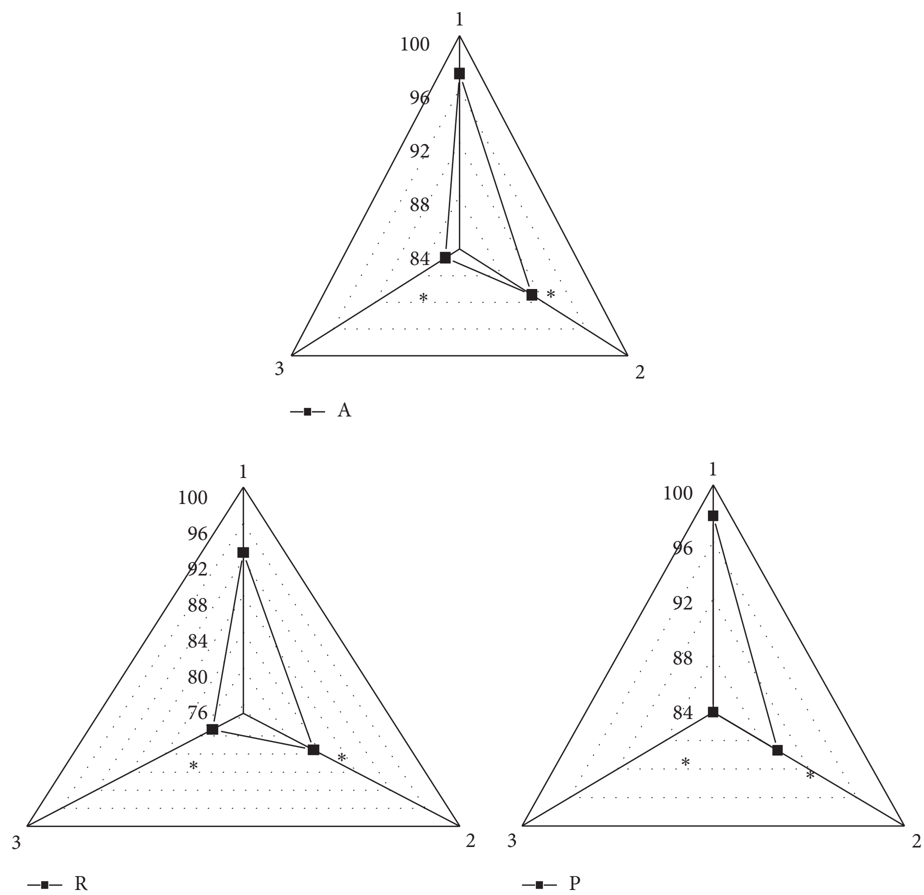

Figure 11: Comparison on segmentation accuracy, precision, and recall of the three algorithms. *Note.* 1 was the algorithm in this study; 2 was the SE-Res Block U-shaped CNN algorithm; 3 was the density peak clustering algorithm. *indicated that the difference compared with 1 was statistically significant $(P < 0.05)$.

postmenopausal volume of the ovary decreases during the sexual maturity [16]. Research shows that ovarian tumor is one of the common tumors of female genitalia [17], and its malignant tumor is the tumor with the highest mortality among gynecological malignancies. According to research reports, the 5-year survival rate has not improved significantly in recent years, but great progress has been made in basic research and clinical diagnosis and treatment of ovarian malignant tumors. The malignant and benign of ovarian tumor affect the choice of treatment options and the

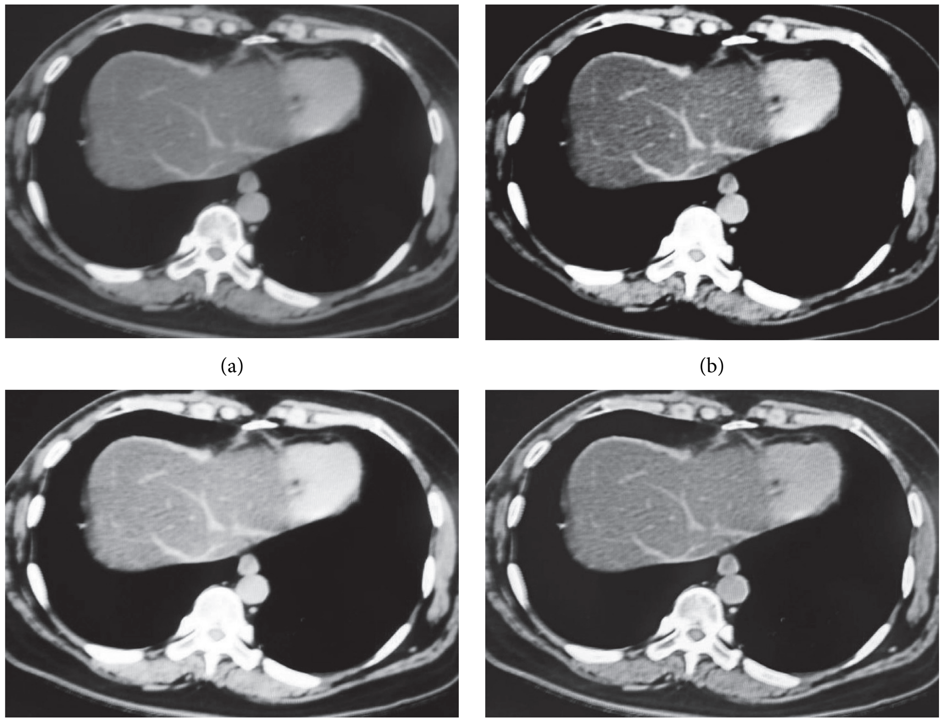

(a) (b) (c) (d)

Figure 12: The breast cancer CT segmentation and reconstruction images of three algorithms. *Note.* (a) Original image; (b) the image after segmented using the algorithm in this study; (c) image segmented using the SE-Res Block U-shaped CNN algorithm; and (d) image segmented with the density peak clustering algorithm.

evaluation of prognosis. Benign ovarian tumors are called ovarian cysts [18]. If it is less than three centimeters, surgery is usually not required, and it can take Jingangteng capsules to inhibit the growth of fibroids; if it is more than 5 cm, laparoscopic surgery should be considered to remove the cyst [19]. The treatment of ovarian malignant tumors is mainly surgery and adjuvant chemotherapy and radiotherapy. For patients with fertility requirements, a full staging operation for ovarian cancer with preserving fertility can be performed. For patients with ovarian malignancies without fertility requirements or late stage [20]. Complete staging or cytoreductive surgery for ovarian cancer is performed directly, and the appendix needs to be removed for special types of malignant tumors. After the surgery, 4–6 courses of chemotherapy are needed, and the patient's physical condition should be considered comprehensively before the surgery.

In this study, 100 patients with ovarian tumor were selected as the research objects. After CT imaging, the patients were subjected to manual evaluation and CNN intelligence algorithm segmentation. The accuracy, precision, and recall of the CNN segmentation method were detected, so as to explore the application of ultrasonic image segmentation technology based on the CNN intelligent algorithms in the diagnosis of ovarian tumor. The results revealed that the numbers of TP were 50, 49, and 50; the numbers of FP were 1, 2, and 1; the numbers of FN were 2, 3, and 2; and the numbers of TN were 47, 46, and 47, respectively. There was almost no difference between the positive and negative cases measured three times ($P \geq 0.05$), indicating that the algorithm model was stable with high effectiveness. The accuracy of the CNN algorithm was 0.97, 0.95, and 0.97, respectively, for the three measurements, indicating that the predictions of malignant tumors and benign tumors were correct; precision was 0.98, 0.96, and 0.98, respectively, which referred to the ratio of predicted malignant tumors accounting for the actually malignant tumors; the recall was 0.96, 0.94, and 0.96, respectively, which referred to the ratio of malignant tumors found. The accuracy, precision, and recall of the three tests were not significant ($P \geq 0.05$), indicating that the CNN algorithm was stable and showed high long-term feasibility. The comprehensive evaluation of a single index was not high, so F-measure was adopted to perform comprehensive evaluation on the data. The larger the value of F, the higher the effectiveness of the algorithm model. The parameter was set to 1 to obtain $F1$, and the three $F1$ values were 0.97, 0.94, and 0.97, respectively. The F values determined by the CNN algorithm for the three times were all close to 100%, which indicated that the algorithm model was very effective, and the difference among the three data was not significant ($P \geq 0.05$), suggesting that the algorithm model showed high stability and can be adapted to long-term clinical applications. Such results were similar to the current research status. The results showed that the accuracy, precision, and recall of CNN intelligence algorithm for CT image segmentation were high. The higher the comprehensive evaluation, the higher the effectiveness, the better the image segmentation effect, and the better diagnostic effect for differentiation of benign and malignant ovarian tumor. The SE-Res Block U-shaped CNN algorithm and the density peak clustering algorithm were introduced to compare with the algorithm in this study. It was found that the segmentation accuracy, precision, and recall rate of the algorithm in this study were significantly greater than those of the SE-Res Block U-shaped CNN algorithm and density peak clustering algorithm ($P < 0.05$). Such results were similar to the research results of Al-Katib et al. [21], indicating that the CNN segmentation algorithm used in this study showed better segmentation performance for CT images than traditional algorithms and had clinical application value.

5. Conclusion

In this study, a CNN intelligence algorithm model was constructed and applied to ovarian tumor CT images to segment the images, so as to explore the application of the algorithm in the clinical analysis of ovarian tumor. The results disclosed that the accuracy, precision, recall, and comprehensive evaluation values of CNN intelligence algorithm for CT image segmentation were all high; the difference among the data results of multiple running was not obvious, so the stability of the system was high, showing better diagnostic effect on differentiation of benign and malignant ovarian tumor. However, the number of selected case samples in this study was small, which may have little impact on the experimental results. In addition, there was a lack of comparison with the segmentation effect of other intelligent algorithms, so that the representativeness was low. Therefore, in the follow-up experimental research, the sample size would be increased, and other algorithms would be used to further analyze the application of segmentation of CT images based on intelligence algorithms in the diagnosis of ovarian tumor. In short, this study provided theoretical guidance and clinical evidence for clinical diagnosis of ovarian tumor and other diseases.

Data Availability

The data used to support the findings of this study are available from the corresponding author upon request.

Conflicts of Interest

The authors declare no conflicts of interest.

References

[1] S. Ren, K. He, R. Girshick, and J. Sun, "R-CNN: towards real-time object detection with region proposal networks," *IEEE Transactions on Pattern Analysis and Machine Intelligence*, vol. 39, no. 6, pp. 1137–1149, 2017.

[2] Z. Wan, Y. Dong, Z. Yu, H. Lv, and Z. Lv, "Semi-supervised support vector machine for digital twins based brain image fusion," *Frontiers in Neuroscience*, vol. 15, Article ID 705323, 2021.

[3] A. Picos and J. M. Peralta-Hernández, "Genetic algorithm and artificial neural network model for prediction of discoloration dye from an electro-oxidation process in a press-type reactor," *Water Science and Technology: A Journal of the International Association on Water Pollution Research*, vol. 78, no. 3-4, pp. 925–935, 2018.

[4] C. Guo, J. Lu, Z. Tian, W. Guo, and A. Darvishan, "Optimization of critical parameters of PEM fuel cell using TLBO-DE based on Elman neural network," *Energy Conversion and Management*, vol. 183, pp. 149–158, 2019.

[5] T. K. Patra, V. Meenakshisundaram, J.-H. Hung, and D. S. Simmons, "Neural-network-biased genetic algorithms for materials design: evolutionary algorithms that learn," *ACS Combinatorial Science*, vol. 19, no. 2, pp. 96–107, 2017.

[6] C. Chen, K. Huang, D. Li, Z. Zhao, and J. Hong, "Multi-segmentation parallel CNN model for estimating assembly torque using surface electromyography signals," *Sensors*, vol. 20, no. 15, p. 4213, 2020.

[7] J. Jiang, L. Zhou, Y. He, X. Jiang, and Y. Fu, "Using stacked neural network to improve the auto-segmentation accuracy of Graves' ophthalmopathy target volumes for radiotherapy," *Sheng Wu Yi Xue Gong Cheng Xue Za Zhi*, vol. 37, no. 4, pp. 670–675, 2020.

[8] Y. Zhang, X. Gao, L. He, W. Lu, and R. He, "Objective video quality assessment combining transfer learning with CNN," *IEEE Transactions on Neural Networks and Learning Systems*, vol. 31, no. 8, pp. 2716–2730, 2020.

[9] H. Zhang, P. Bai, Z. Guo et al., "An algorithm for three-dimensional plumonary parenchymal segmentation by integrating surfacelet transform with pulse coupled neural network," *Sheng Wu Yi Xue Gong Cheng Xue Za Zhi*, vol. 37, no. 4, pp. 630–640, 2020.

[10] S. Xie, Z. Yu, and Z. Lv, "Multi-disease prediction based on deep learning: a survey," *Computer Modeling in Engineering and Sciences*, vol. 127, no. 3, pp. 1–34, 2021.

[11] Z.-Q. K. Tian and D. Zhou, "Exponential time differencing algorithm for pulse-coupled Hodgkin-Huxley neural networks," *Frontiers in Computational Neuroscience*, vol. 14, p. 40, 2020.

[12] H. Wang, T. Zhao, L. C. Li et al., "A hybrid CNN feature model for pulmonary nodule malignancy risk differentiation," *Journal of X-Ray Science and Technology*, vol. 26, no. 2, pp. 171–187, 2018.

[13] H. Song, W. W. Yang, W. Yang, S. Dai, L. Du, and Y. Sun, "Using dual-channel CNN to classify hyperspectral image based on spatial-spectral information," *Mathematical Biosciences and Engineering*, vol. 17, no. 4, pp. 3450–3477, 2020.

[14] S. Nougaret, Y. Lakhman, N. Molinari et al., "CT features of ovarian tumors: defining key differences between serous borderline tumors and low-grade serous carcinomas," *American Journal of Roentgenology*, vol. 210, no. 4, pp. 918–926, 2018.

[15] B. D. O'Leary, T. Treacy, T. Geoghegan, T. A. Walsh, W. D. Boyd, and D. J. Brennan, "Incidental thoracic findings on routine computed tomography in epithelial ovarian cancer," *International Journal of Gynecological Cancer*, vol. 28, no. 6, pp. 1073–1076, 2018.

[16] A. Gadducci, E. Simonetti, G. Manca et al., "Positron emission tomography/computed tomography in platinum-sensitive recurrent ovarian cancer: a single-center Italian study," *Anticancer Research*, vol. 40, no. 4, pp. 2191–2197, 2020.

[17] L. Baandrup, M. T. Faber, G. L. Aalborg, and S. K. Kjaer, "Borderline ovarian tumors in Denmark 1997–2018: time trends in incidence by histology, age and educational level," *Acta Obstetricia et Gynecologica Scandinavica*, vol. 100, no. 3, pp. 436–443, 2021.

[18] R. S. Suidan, P. T. Ramirez, D. M. Sarasohn et al., “A multicenter assessment of the ability of preoperative computed tomography scan and CA-125 to predict gross residual disease at primary debulking for advanced epithelial ovarian cancer,” *Gynecologic Oncology*, vol. 145, no. 1, pp. 27–31, 2017.

[19] H. Lu, M. Arshad, A. Thornton et al., “A mathematical-descriptor of tumor-mesoscopic-structure from computed-tomography images annotates prognostic- and molecular-phenotypes of epithelial ovarian cancer,” *Nature Communications*, vol. 10, no. 1, p. 764, 2019.

[20] C. Dolci, L. Ceppi, L. Guerra et al., “Role of 18F-fluoro-2-deoxyglucose positron emission tomography/computed tomography (18F-FDG PET/CT) in malignant ovarian germ cell tumors: a single-center experience with long term follow-up,” *International Journal of Gynecological Cancer*, vol. 29, no. 8, pp. 1298–1303, 2019.

[21] S. Al-Katib, G. Gupta, A. Brudvik, S. Ries, J. Krauss, and M. Farah, “A practical guide to managing CT findings in the breast,” *Clinical Imaging*, vol. 60, no. 2, pp. 274–282, 2020.